

DESY 96/168  
hep-ph/9608401

# The Total Cross Section and the BFKL Pomeron at $e^+e^-$ Colliders

J. Bartels<sup>a</sup>, A. De Roeck<sup>b</sup> and H. Lotter<sup>a</sup>

<sup>a</sup> II. Institut f. Theoretische Physik, Universität Hamburg, Lunper Chaussee 149,  
D-22761 Hamburg <sup>1</sup>

<sup>b</sup> Deutsches Elektronen-Synchrotron, DESY, Notkestr.85, D-22603 Hamburg

We present a numerical estimate of the total cross section at LEP and at the designed  $e^+e^-$  Next Linear Collider (NLC), based upon the BFKL Pomeron. We find for the linear collider that the event rate is substantial provided electrons scattered under small angles can be detected, and a measurement of this cross section provides an excellent test of the BFKL Pomeron. For LEP, although the number of events is substantially smaller, an initial study of this process is feasible.

---

<sup>1</sup>Supported by Bundesministerium für Forschung und Technologie, Bonn, Germany under Contract 05 6H H 93P (5) and EEC Program "Human Capital and Mobility" through Network "Physics at High Energy Colliders" under Contract CHRX-CT 93-0357 (DG12 COMA).

1. Recently much attention has been given to the BFKL Pomeron [1], in particular in the context of small- $x$  deep inelastic electron proton scattering at HERA. Whereas the use of this QCD leading logarithmic approximation for the proton structure function is affected by serious theoretical difficulties, it has been argued [2] that the observation of forward jets near the proton beam provides a much more reliable test of the BFKL Pomeron. The main reason for this lies in the fact that the forward jet cross section involves only a single large momentum scale, namely the transverse momentum of the forward jet which is chosen to be equal or close to the virtuality of the photon. In the structure function  $F_2$ , on the other hand, the BFKL Pomeron feels both the large momentum scale of the photon mass and the lower factorization scale. In addition, the diffusion in  $\log k_T^2$  always leads to a nonzero contribution of small transverse momenta where the use of the leading logarithmic approximation becomes doubtful. A numerical estimate shows that for the forward jets at HERA [3] the contribution from this dangerous infrared region is reasonably small, whereas in the case of  $F_2$  [4] the situation is much less favorable. As to the experimental situation, a recent analysis of HERA data [5, 6] on the production of forward jets shows a very encouraging agreement between data and the theoretical prediction.

In this note we would like to point out that also  $e^+e^-$  linear colliders, in particular the linear colliders with a rather high luminosity, offer an excellent opportunity to test the BFKL prediction. The process to be looked at is the total cross section of  $\gamma\gamma$  scattering. The measurement of this cross section requires the double tagging of both outgoing leptons close to the forward direction. By varying the energy of the tagged leptons it is possible to probe the total cross section of the subprocess  $\gamma\gamma \rightarrow \gamma\gamma$  from low energies up to almost the full energy of the  $e^+e^-$  collider. For sufficiently large photon virtualities we again have a situation with only large momentum scales. In other words, photons with large virtualities are objects with small transverse sizes, and it is exactly this situation for which the BFKL approximation should be considered to be most reliable. The energy dependence of this cross section, therefore, should be described by the power law of the BFKL Pomeron.

From the theoretical point of view it is clear that we want the photon masses to be large. On the other hand, because of the photon propagators, the  $e^+e^-$  cross section for this final state (i.e. the event rate for the process under discussion) falls off very rapidly with increasing photon masses. Therefore, one cannot afford to have too large photon virtualities. As a compromise, we chose the range of 5 to 200  $\text{GeV}^2$  (for experimental considerations see further below). As to the energies of the  $\gamma\gamma$  subprocess, we can in principle go up to almost the full collider energies. From the theoretical side, however, it is important to estimate the diffusion in the internal transverse momenta  $k_T$ . In the center of the BFKL ladders (Fig.1), the distribution in  $\log k_T^2$  is given by a Gaussian, with center at  $\log Q^2$  (if we chose, for simplicity, both photon virtualities to be equal), and with the width growing linearly with the square root of the rapidity. As soon as the small- $k_T$  part of the gaussian reaches the confinement region the BFKL prediction (which is based upon a leading-log calculation) becomes unreliable. Corrections to the BFKL pomeron, in particular those which are expected to restore unitarity are no longer small. Qualitatively they are expected to reduce the growth of the cross section with increasing energy. Below we will argue that, at least for the linear collider, this energy region can be reached. In other words, at highest energies for the  $\gamma\gamma$  subprocess, a deviation from the power-rise of the BFKL Pomeron might become visible.

2. The theoretical prediction of the cross section is based on the high energy behavior of the

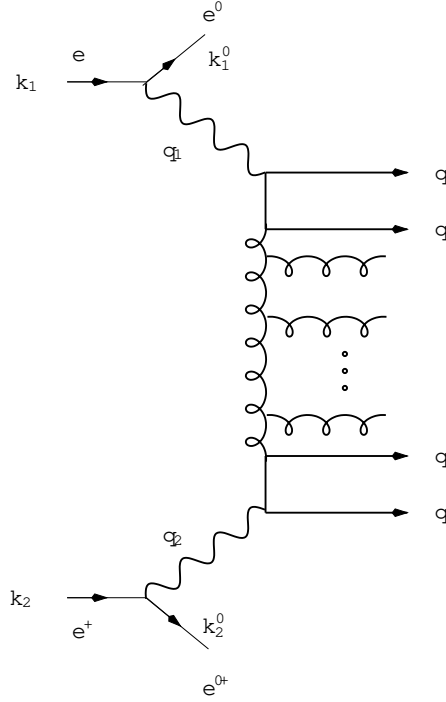


Figure 1: Feynman diagram for the process  $e^+ e^- \rightarrow e^+ e^- + \text{anything}$ .

diagrams shown in Fig. 1. Let us first define suitable variables. In analogy to DIS kinematics we chose the scaling variables

$$y_1 = \frac{q_1 k_2}{k_1 k_2}; \quad y_2 = \frac{q_2 k_1}{k_1 k_2} \quad (1)$$

and

$$x_1 = \frac{Q_1^2}{2q_1 k_2}; \quad x_2 = \frac{Q_2^2}{2q_2 k_1} \quad (2)$$

where the photon virtualities are, as usual,  $Q_i^2 = -q_i^2$ ,  $i = 1, 2$ . Energies are denoted by  $s = (k_1 + k_2)^2$  and  $\hat{s} = (q_1 + q_2)^2 = sy_1 y_2$ . With our definitions of the scaling variables we have  $Q_i^2 = sx_i y_i$ ,  $i = 1, 2$ . We consider the limit of large  $Q_1^2, Q_2^2$ , and  $\hat{s}$  with

$$Q_1^2; Q_2^2 \sim \hat{s} \quad (3)$$

The calculation is straightforward and, neglecting terms of the order of  $Q_i^2/\hat{s}$ , leads to the following result:

$$\frac{d\sigma_{e^+ e^-}}{dQ_1^2 dQ_2^2 dy_1 dy_2} = \frac{\alpha_{em}^2}{16 y_1 Q_1^4} \frac{\alpha_{em}^2}{16 y_2 Q_2^4} \int \frac{d^2 \mathbf{q}}{2^2} \exp[4 \log s \frac{y_1 y_2}{Q_1^2 Q_2^2}] \quad (5)$$

$$\times \left[ (1 - y_1) W_L^{(1)}(\mathbf{q}) + \frac{1 + (1 - y_1)^2}{2} W_T^{(1)}(\mathbf{q}) \right] \left[ (1 - y_2) W_L^{(2)}(\mathbf{q}) + \frac{1 + (1 - y_2)^2}{2} W_T^{(2)}(\mathbf{q}) \right] \quad (4)$$

with  $(\gamma) = N_c s = [2(1) \quad (1=2+i) \quad (1=2-i)]$  and we have introduced the invariant functions:

$$W_L^{(i)}(\gamma) = \sum_f q_f^2 s^{-2P-\frac{2}{2}} 8^{\frac{2}{2}+\frac{1}{4}} \frac{\sinh}{\cosh^2} (Q_i^2)^{\frac{1}{2}+i} \quad (5)$$

$$W_T^{(i)}(\gamma) = \sum_f q_f^2 s^{-2P-\frac{2}{2}} 4^{\frac{2}{2}+\frac{9}{4}} \frac{\sinh}{\cosh^2} (Q_i^2)^{\frac{1}{2}+i} \quad (6)$$

Here  $q_f$  is the quark charge, and in our calculations the sum over the flavours goes up to three. For the scale of the first order strong coupling constant we use  $Q_1^2 Q_2^2 (s(M_Z^2) = 0.12)$ . In the high energy limit one can use the saddle point approximation near  $\gamma = 0$  and obtain the following approximation:

$$\begin{aligned} \frac{d e^+ e^-}{dQ_1^2 dQ_2^2 dy_1 dy_2} &= \frac{2_{em}}{16 Y_1 Q_1^4} \frac{2_{em}}{16 Y_2 Q_2^4} \exp \log \frac{s}{s_0} 4 \log \frac{N_c s}{2} \frac{e^{\frac{\log Q_1^2 - Q_2^2}{N_c s} = \frac{56}{(3)} \log s = s_0}}{N_c s = 14 (3) \log s = s_0} \\ &\quad \frac{1}{2^{P-3}} \sum_f q_f^2 Q_1^2 Q_2^2 e^{\sum_f q_f^2 s^{-2P-\frac{2}{2}} A} \\ &\quad " (1 - Y_1) W_{L,0} + \frac{1 + (1 - Y_1)^2}{2} W_{T,0} " \quad " (1 - Y_2) W_{L,0} + \frac{1 + (1 - Y_2)^2}{2} W_{T,0} " \quad (7) \end{aligned}$$

where the constants  $W_{L,0}$ ;  $W_{T,0}$  and  $s_0$  are:

$$s_0 = \frac{q \frac{Q_1^2 Q_2^2}{Y_1 Y_2}}{2^{P-3}} \quad (8)$$

$$W_{L,0} = 2; W_{T,0} = 9: \quad (9)$$

Before we turn to the discussion of numerical results, let us estimate the diffusion of internal transverse momenta into the infrared region. In the center of the BFKL ladders (g.l), the width of the gaussian distribution of  $\log k_T^2$  is given by [3]

$$= \frac{q \frac{s}{(\log k_T^2 - \langle \log k_T^2 \rangle)^2}}{7 \frac{N_c s}{(3) \log s = s_0}} \quad (10)$$

For a typical value  $Q_1^2 = Q_2^2 = 10 \text{ GeV}^2$ , and  $s = 0.22$  one finds, for the maximal value  $Y = \log s = s_0 = 10$  at the NLC,  $\gamma = 4.2$  which means that the diffusion reaches down to  $k_T^2 = 0.15 \text{ GeV}^2$ . For LEP the maximal value for  $Y$  is near 6, and we obtain  $\gamma = 3.2$  and  $k_T^2 = 0.4 \text{ GeV}^2$ . Compared to the forward jets at HERA [3] where the corresponding value lies above  $1 \text{ GeV}^2$ , we now have to expect a substantially larger contribution from the small- $k_T$  region: this should lead to a lowering of the BFKL power behavior of the cross section. In other words, one might be able to see the onset of unitarity corrections to the BFKL Pomeron.

3. Starting from eqs. (4) - (6) we have calculated the differential cross section for different values of the logarithm of the subenergy  $Y = \log s = s_0$ . In order to illustrate the BFKL power law, we have

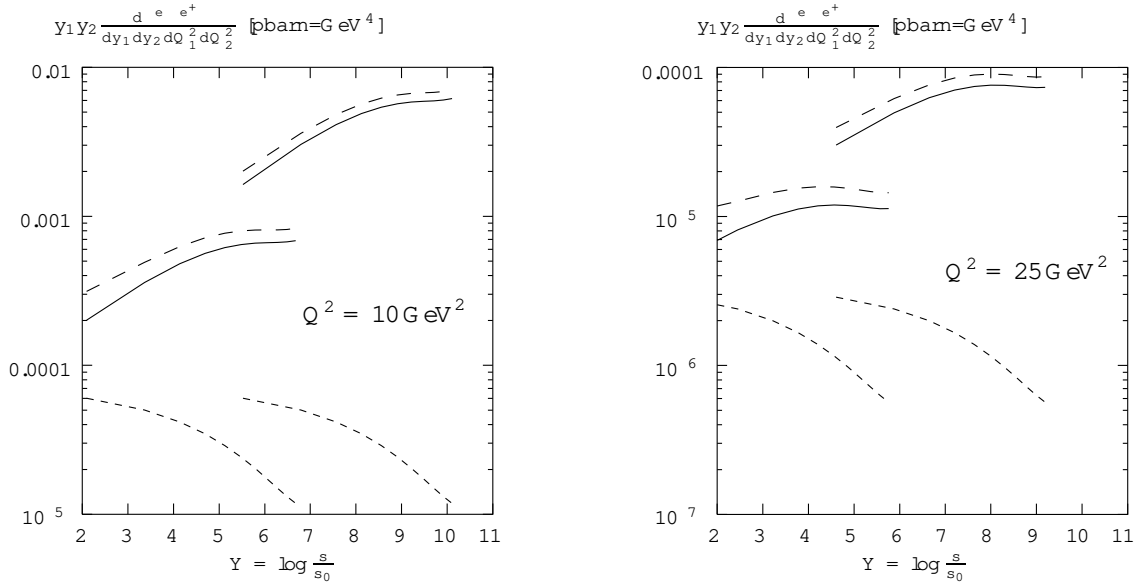


Figure 2: The differential  $e^+e^-$  cross section, multiplied by  $y_1 y_2$ , as a function of the rapidity  $Y = \log s/s_0$ . The full curves denote the exact numerical calculation based upon eq. (4), the dashed curves belong to the analytic high energy approximation (7), and the dotted lines represent the Bom approximation (no gluon production between the two quark pairs). The three curves on the left in each figure belong to LEP, the ones on the right to the Next Linear Collider NLC. We have chosen  $y_1 = y_2$  and  $Q_1^2 = Q_2^2 = 10 \text{ GeV}^2$  (left hand figure) resp.  $Q_1^2 = Q_2^2 = 25 \text{ GeV}^2$  (right hand figure).

multiplied the cross section by  $y_1 y_2$ . In fig. 2 we show the results for both LEP (at the  $Z^0$  mass) and the 500 GeV Next Linear Collider. On the left hand side we display the  $e^+e^-$  cross section for  $Q_1^2 = Q_2^2 = 10 \text{ GeV}^2$ . The right hand side shows the cross section for  $Q_1^2 = Q_2^2 = 25 \text{ GeV}^2$ . The full curves represent the "exact" results based upon (4) - (6), the dashed lines show the "analytic" prediction of eq. (7), and the dashed dotted lines denote the "Bom" approximation (no gluon production between the two fermion pairs). For the exact in the analytic curves one recognizes the BFKL power-like energy behavior, but there is some damping at large rapidity (large  $y_i$ ) due to the photon flux factors in (4) and (7). In the Bom cross section this effect even leads to a decrease of the  $e^+e^-$  cross section at large rapidity  $Y$ . The BFKL predictions are well above the Bom curves, up to more than an order of magnitude. For illustration we show not only the exact but also the analytic calculation in order to demonstrate that for our present purposes the high energy approximation (7) provides a rather good estimate. The exact and the analytical calculations agree up to, typically, a factor less than two. Complete agreement between the exact calculation and the approximation will be reached only at asymptotically high energies. Comparing the right hand side of fig. 2 with the left hand side we find that by increasing  $Q^2$  from 10 to  $25 \text{ GeV}^2$  the cross section decreases by two orders of magnitude. As seen from (4) or (7), the cross section scales with  $1/Q^6$ , and there is an additional decrease at larger  $Q^2$  due to the  $Q^2$ -dependence of  $s(Q^2)$ . Event rates for the NLC and for LEP are shown in fig. 3, taking  $3 \cdot 10^7 \text{ s/year}$ . Due to the limit in time of data taking periods, experiment and accelerator efficiency, this cor-

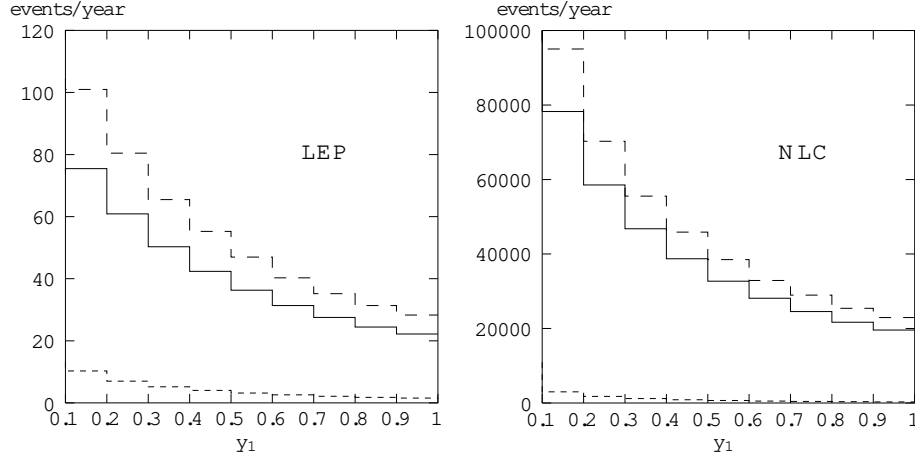


Figure 3: The total number of events per year, as a function of  $y_1$ . The variables  $Q_1^2$  ( $5 < Q_1^2 < 200 \text{ GeV}^2$ ) and  $y_2$  ( $0.1 < y_2 < 0.9$ ) are integrated. The left hand side corresponds to the LEP and the right hand side to the NLC situation. The solid curve shows the results of the exact calculation, the dashed curve shows the approximation and the dotted curve represents the Born result.

responds effectively to several years of operation of the accelerator. In  $Q_1^2$  and  $Q_2^2$  we integrate from 5 to  $200 \text{ GeV}^2$ , and for the  $y_1$ -variable we have chosen 9 bins, as indicated in the figure. The other  $y$ -variable is integrated from 0.1 to 1.0. The rapidity of the subprocess is restricted by  $\log s = s_0 > 2$ . For the luminosities of LEP and of the NLC we have used  $L = 10^{31} \text{ cm}^2 \text{ s}^{-1}$  and  $L = 10^{33} \text{ cm}^2 \text{ s}^{-1}$ , respectively. The event rate calculations are based upon Monte Carlo integration of the phase space, and the accuracy is of the order of 5%. The difference of the event rates between the NLC and LEP is a consequence of both the higher luminosity and the higher energy of the NLC.

4. Due to experimental restrictions, however, these event rates can only give a first impression and not more. The measurement of the total cross section of scattering can be made at existing and future  $e^+e^-$  colliders using so called "double tag" events. These are events where both outgoing leptons are detected and some hadronic activity is observed in the central detector. The  $Q^2$  value of the virtual photon emitted from the lepton is  $Q^2 = 2E_b E_{\text{tag}} (1 - \cos \theta_{\text{tag}}) = 4E_b E_{\text{tag}} \sin^2 \frac{\theta_{\text{tag}}}{2}$ , with  $E_{\text{tag}}$  and  $\theta_{\text{tag}}$  the energy and angle of the tagged lepton, and  $E_b$  the energy of the incident lepton. The variable  $y$  is given by  $y = 1 - (E_{\text{tag}}/E_b) \cos^2 \frac{\theta_{\text{tag}}}{2}$ . Combination of the two relations leads to the convenient equation

$$Q^2 = 4E_b^2 (1 - y) \tan^2 \frac{\theta_{\text{tag}}}{2} \quad (11)$$

which holds for any of the two incoming leptons. Experiments at LEP tag electrons down about 60 mrad [7, 8] leading to  $Q^2$  values as low as to  $5 - 6 \text{ GeV}^2$ . In order to reach such  $Q^2$  values at a NLC with a CMS energy of 500 GeV, the scattered leptons need to be detected down to 10 mrad. For photons of virtuality  $20 \text{ GeV}^2$  angles down to about 15-20 mrad need to be covered. Present preliminary detector designs intent to tag electrons only above 100-150 mrad [10], leading to minimum reachable  $Q^2$  values in the range of 100 -  $200 \text{ GeV}^2$ . One of the main problems at small angles is  $e^+e^-$  pair production, but preliminary studies indicate that angles down to 20 mrad

are within reach [9]. The  $y$  values reached in present single tagged analysis at LEP, are in the range  $y < 0.25$ . However using double tagged events the background should be kept well under control also for larger  $y$  values, and therefore values of  $y = 0.5$  or more, which lead to a large mass system for the hadronic final state and, correspondingly, to an extended ladder, are a realistic goal.

In order to incorporate these conditions into our calculation of event rates, we have repeated

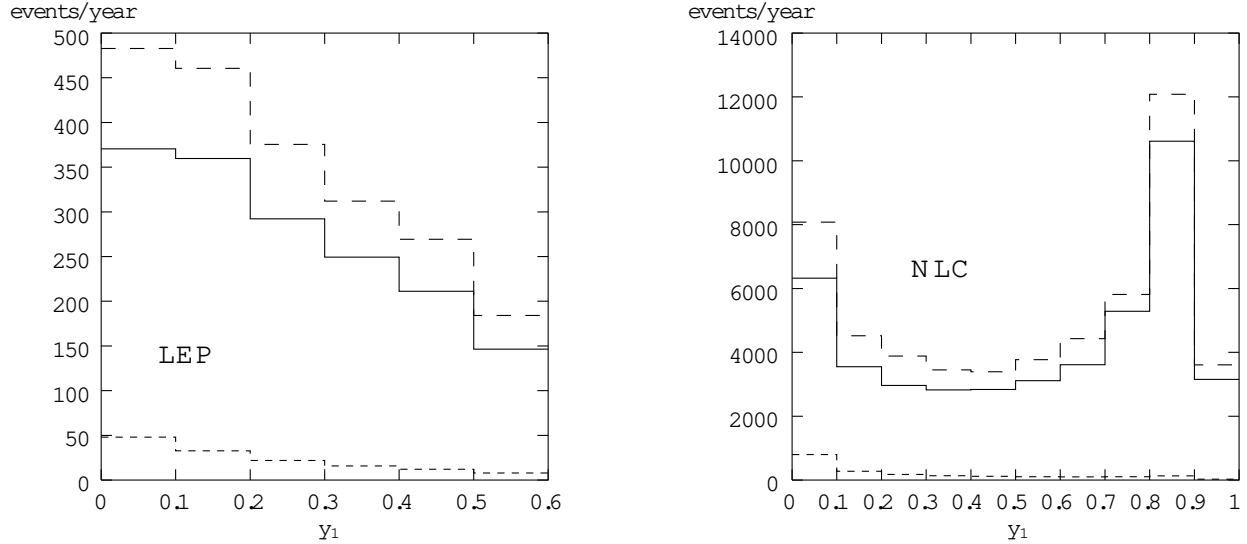


Figure 4a: The total number of events per year (3  $\cdot 10^5$ s) with detector cuts in angle taken into account. We have chosen  $E_{\text{tag}} > 20 \text{ GeV}$ ,  $\log s = s_0 > 2$ ,  $2.5 < Q_i^2 < 200 \text{ GeV}^2$ . The acceptance cut is  $\theta_{\text{tag}} > 20 \text{ m rad}$ . The  $y$ -binning is the same as in fig. 3 and we have LEP on the left and NLC on the right hand side.

the previous calculations with more realistic kinematical cuts. For both the NLC and LEP we impose the constraints  $\theta_{\text{tag}} > 20 \text{ m rad}$  (fig. 4a) and  $\theta_{\text{tag}} > 60 \text{ m rad}$  (fig. 4b), and we require  $E_{\text{tag}} > 20 \text{ GeV}$  (i.e. approximately  $y_1 < 0.9$  for the NLC and  $y_1 < 0.6$  for LEP). Further restrictions are  $2.5 < Q_i^2 < 200 \text{ GeV}^2$  and  $\log s = s_0 > 2$ . For the NLC case, in particular for smaller  $y_1$ , the event rate is substantially lower than in fig. 3, indicating the importance of the detector angle cut. Clearly,  $\theta_{\text{tag}} = 20 \text{ m rad}$  looks highly desirable for both machines. For LEP, the comparison with the NLC now looks more favorable than in fig. 3. If  $\theta_{\text{tag}}$  can be taken down to  $20 \text{ m rad}$ , the NLC rate is clearly substantially larger than the LEP rate. For  $\theta_{\text{tag}} = 60 \text{ m rad}$ , however, the  $Q^2$  values at the NLC are considerably larger than those at LEP (cf. eq. (11)), and the small  $y$  region in the right hand diagram in fig. 4b has very few events. This explains why, despite the higher energies and the larger luminosity of the NLC, LEP is doing better than the NLC.

Finally, we have computed a few integrated event rates. The results are shown in Table 1 for the NLC, LEP-90 and LEP-180. We integrated  $2.5 < Q_i^2 < 200 \text{ GeV}^2$ ,  $0.1 < y_1 < 1.0$ , with the constraints  $E_{\text{tag}} > 20 \text{ GeV}$ ,  $\log s = s_0 > 2$ , and for the detector angles we have chosen  $\theta_{\text{tag}} > 20 \text{ m rad}$ ,  $60 \text{ m rad}$ , and  $100 \text{ m rad}$ . For the smallest angles the ratio of BFKL to Born cross section is larger than a factor of 75 for the NLC, while it is reduced to 25 at LEP-90. For angles above  $60 \text{ m rad}$  for

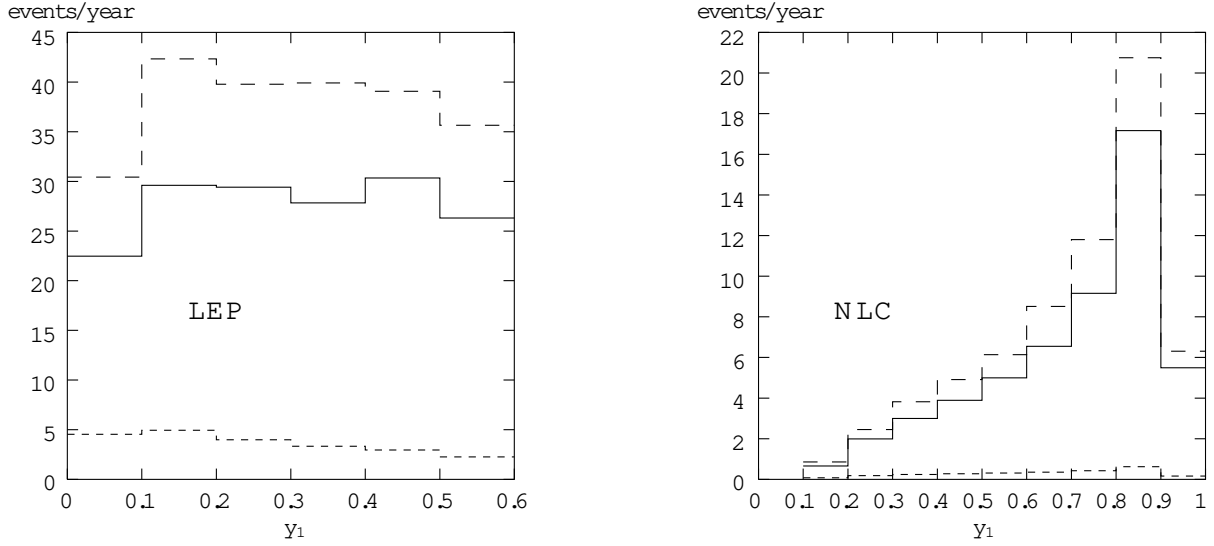


Figure 4b: The same as in Fig. 4a but with acceptance cut  $\theta_{\text{tag}} > 60 \text{ m rad}$ .

exact	analytic	Bom	$\theta_{\text{tag}}; \text{m rad}$	
29500	36400	495	20 m rad	NLC
51	68	2	60 m rad	
1	1	0	100 m rad	
940	1150	47	20 m rad	LEP-90
120	158	13	60 m rad	
11	15	2	100 m rad	
3250	3870	53	20 m rad	LEP-180
750	880	13	30 m rad	
24	30	3	60 m rad	
2	3	0	100 m rad	

Table 1: Total event rates per year for NLC, LEP I and LEP II.

which single tag measurements at LEP exist, the BFKL cross section is by a factor of 10 larger than the Bom cross section. This factor is larger at the NLC, but the limitation in  $Q^2$  strongly affects the rate as discussed above. The total number of events produced in the four LEP experiments together at LEP-90, taking a total collected integrated luminosity of  $150 \text{ pb}^{-1}/\text{experiment}$  is twice the number of events given in Table 1. Conversely, the LEP-180 numbers correspond to a total number of events collected by the experiments if  $75 \text{ pb}^{-1}$  will be delivered by the machine. The experiments at LEP-180 are foreseen to measure already now down to angles about 30 m rad. Table 1 shows that the event rate for this angle is reasonable. We conclude that, mainly because of the higher luminosity of the NLC, such a machine offers an excellent possibility to observe the BFKL Pomeron, provided the detectors can be improved to reach small angles down to about 20 m rad. For LEP the total event rate looks less encouraging, but it is still worthwhile to pursue further



studies in this direction.

5. In summary, we have estimated the total cross section of  $\gamma\gamma$  scattering at both LEP and the NLC. At high energies, this subprocess is dominated by the BFKL Pomeron and therefore provides an ideal test of this QCD calculation. A rough estimate of the diffusion in  $\log k_T^2$  shows that, at the high energy tail of this subprocess, corrections to the BFKL become non-negligible, and hence deviations from the BFKL power law may become visible.

For a realistic estimate of the number of observable events we find a strong dependence on detector restrictions. In order to have a sufficiently large number of events it is necessary to tag both leptons close to the beam direction; a desirable angle would be 20 mrad, and energies of the tagged leptons should go down to about 20 GeV. In this region the NLC provides an excellent possibility for testing the BFKL Pomeron. For LEP (in particular at 90 GeV lepton energies) the number of events is still sufficiently large to justify a dedicated search. For larger angles (e.g. 60 mrad) the NLC loses in the number of events, faster than LEP.

Acknowledgements: We wish to thank Peter Zerwas, Daniel Schulte and Richard Nisius for very helpful discussions.

Note added: Results similar to those contained in this paper have been obtained independently by S. Brodsky, F. Hautmann and D. Soper [11].

## References

- [1] E.A. Kuraev, L.N. Lipatov and V.S. Fadin, Sov.Phys.JETP 45 (1977) 199;  
Ia.Ia. Balitski and L.N. Lipatov, Sov.J.Nucl.Phys. 28 (1978) 822.
- [2] A.H. Mueller, Nucl.Phys.B (Proc.Suppl.) 18C (1991) 125;  
J.Bartels, A.DeRoeck and M.Loewe, Z.Phys.C 54 (1992) 635;  
J.Bartels, M.Besancon, A.DeRoeck and J.Kurzhofer, in Proceedings of the HERA Workshop 1991 (eds W.Buchmuller and G.Ingelman), p.203;  
J.Kwiecinski, A.D.Martin and P.J.Sutton, Phys.Lett. B 287 (1992) 254; Phys.Rev. D 46 (1992) 921;  
W.-K.Tang, Phys.Lett. B 278 (1991) 363.
- [3] J.Bartels and H.Lotter, Phys.Lett. B 309 (1993) 400.
- [4] J.Bartels, H.Lotter and M.Vogt, Phys.Lett. B 373 (1996) 215.
- [5] J.Bartels, V.DeDuca, A.DeRoeck, D.Graudenz and M.Wuestho, DESY-96-36, CERN-TH/96-83, ANL-HEP-PR-96-23, Edinburgh-96-2 (to be published in Phys.Lett. B).
- [6] A.DeRoeck, to appear in the proceedings of the DIS96 Workshop, Rome, April (1996).
- [7] DELPHI Collaboration, Contributed paper to the ICHEP 96 conference at Warsaw, pa02-21.
- [8] OPAL Collaboration, Contributed paper to the ICHEP 96 conference at Warsaw, pa03-09.
- [9] D.Schulte, PhD Thesis Hamburg 1996, in litt.

- [10] Physics and Technology of the Next Linear Collider, SLAC report 485.
- [11] S.Brodsky, F.Hautmann and D.Soper, Talk presented by F.Hautmann at the ICHEP 96 conference at Warsaw .